

15 **The largest rates of Antarctic glacial ice mass loss are occurring to the west of the**
16 **Antarctica Peninsula in regions where warming of subsurface continental shelf**
17 **waters is also largest. However, the physical mechanisms responsible for this**
18 **warming remain unknown. Here we show how localized changes in coastal winds off**
19 **East Antarctica can produce significant subsurface temperature anomalies ($>2^{\circ}\text{C}$)**
20 **around much of the continent. We demonstrate how coastal-trapped barotropic**
21 **Kelvin waves communicate the wind disturbance around the Antarctic coastline. The**
22 **warming is focused on the western flank of the Antarctic Peninsula because the**
23 **circulation induced by the coastal-trapped waves is intensified by the steep**
24 **continental slope there, and because of the presence of pre-existing warm subsurface**
25 **water offshore. The adjustment to the coastal-trapped waves shoals the subsurface**
26 **isotherms and brings warm deep water upwards onto the continental shelf and closer**
27 **to the coast. This result demonstrates the vulnerability of the West Antarctic region**
28 **to a changing climate.**

29 The rate of global sea level rise between 1993-2010 is estimated to have increased
30 by $\sim 150\%$ relative to the 1901-1990 average rate¹. The flow of grounded Antarctic glacial
31 ice into the ocean contributed $\sim 28\%$ to global sea level rise between 1960-2004, and its
32 contribution is likely to increase². From 2003-2014 the rate of West Antarctic ice mass
33 loss has doubled³, while from 1996-2013 the Totten Glacier in East Antarctica thinned by
34 ~ 12 m at the grounding line⁴ (i.e. the point where the ice sheet starts to float). Antarctic
35 glacial ice loss is primarily influenced by ocean-ice interactions at the base of the floating
36 ice shelves where basal melt rates are estimated to increase by ~ 10 m/yr for a 1°C increase
37 in ocean temperatures^{5,6}. The focus of this study is on the mechanisms that give rise to
38 subsurface ocean warming around the Antarctic continental margin⁷. Future contributions
39 from Antarctic ice sheets are the largest source of uncertainty in sea level projections

40 because many Antarctic ice sheets are hypothesized to become rapidly unstable when
41 warmer ocean water causes the ice sheet grounding line to retreat^{8,9,10}. Recent estimates
42 suggest Antarctica could contribute >1 m of sea level rise by 2100 and > 15 m by 2500¹¹.

43 Constraining Antarctica's contribution to global sea level rise requires
44 understanding the water mass interactions across the near-circumpolar Antarctic Slope
45 Front. This front separates the cold, fresh waters on the continental shelf from the warmer,
46 saltier Circumpolar Deep Water generally found offshore¹². Antarctic coastal ocean
47 observations suggest warming of 0.1-0.3 °C/decade since 1990 on the continental shelves
48 of the Bellingshausen Sea and Amundsen Sea and along the western side of the Antarctica
49 Peninsula⁷. This warming is linked with a shallowing of the mid-depth temperature
50 maximum over the continental slope and shelf that allows the warmer offshore water to
51 flow onshore. The warming trends positively correlate with observed estimates of rapidly
52 increasing rates of glacial ice mass loss since the 1990s^{13,14}.

53 The mechanisms responsible for the observed warming of West Antarctic
54 continental shelf waters remain highly uncertain. Some studies suggest a positive trend in
55 the Southern Annular Mode (SAM), associated with strengthened and poleward shifted
56 Southern Hemisphere mid-latitude winds¹⁵, can aid the intrusion of warm offshore waters
57 onto the Antarctic continental shelf. For example, *in-situ* Bellinghausen Sea observations
58 spanning the summer seasons from 1993-2004 highlight a large coastal intrusion of
59 offshore subsurface waters that is correlated with a positive SAM index¹⁶. A mesoscale
60 eddy-permitting ocean model also demonstrated how SAM-induced wind changes can
61 generate subsurface Antarctic coastal warming by anomalous shallowing of isotherms¹⁷.
62 Finer resolution regional and idealized ocean model studies propose that the transport of
63 heat across the Antarctic Slope Front can also be driven by mesoscale eddies^{18,19} and
64 tides²⁰.

65 The positive SAM trend observed since the 1950s is projected to persist through
66 the 21st Century²¹, raising concerns that it may lead to increased basal melt rates from
67 anomalous intrusion of warm Circumpolar Deep Water onto the shelf. Prior studies have
68 largely focussed on the direct local impacts of changing winds on the Antarctic coastal
69 ocean temperature structure^{17,18,19}. However, observed subsurface coastal warming has
70 been most rapid on the western side of the Antarctic Peninsula⁷, despite evidence that the
71 influence of the SAM on the coastal winds is largest in East Antarctica (Fig. 1a, Fig. S1).
72 Here we seek to understand why the strongest warming of Antarctic subsurface coastal
73 waters appears west of the Antarctic Peninsula. We propose that the warming to west of
74 the Antarctic Peninsula can be forced by changes in remote Antarctic coastal winds.

75

76 **Coastal ocean response to East Antarctic winds**

77 Our experimental design is based on a previous study wherein a positive SAM
78 wind perturbation applied along the entire Antarctic coastline creates near-circumpolar
79 warming ($>2^{\circ}\text{C}$) of the subsurface (200-700m depth) coastal waters¹⁷. The warming in that
80 study was attributed to the anomalous intrusion of warm Circumpolar Deep Water onto
81 the shelf in response to the reduction in coastal surface Ekman pumping due to the local
82 wind change. Here, unlike the previous study, the positive SAM wind perturbation is only
83 applied along the East Antarctic coastline between 20°E-120°E (Fig. 1a,b; Methods). The
84 effect of this East Antarctic wind perturbation is investigated with two global ocean, sea-
85 ice models (known as MOM01 and MOM025) that differ only in the resolution of their
86 vertical and horizontal grids. MOM01 (MOM025) has ~4.5 km (~11 km) horizontal grid
87 spacing at 65°S and 75 (50) vertical levels. The perturbation responses are qualitatively
88 consistent between MOM025 and MOM01 in that the signs of change are robust.
89 Quantitative differences between the two models help to constrain the forcing response

90 and the mechanisms responsible.

91 The East Antarctic wind perturbation produces both local and remote impacts
92 along the Antarctic continental margin. Firstly, it causes a circumpolar decrease in
93 Antarctic coastal sea level that is amplified as the perturbation persists. After one year sea
94 level falls by ~6 cm in the East Antarctic perturbation region, and 1-2 cm on the western
95 side of the Antarctic Peninsula over 6000 km away (Fig. 1c). By year 5 sea level has
96 dropped by ~15 cm in the wind perturbation region, and ~10 cm west of the peninsula. In
97 the previous study where the same wind perturbation was applied over the entire Antarctic
98 coastline, a similar circumpolar drop in coastal sea level was attributed to a reduction in
99 local wind-driven onshore surface Ekman transport¹⁷. Here, surface Ekman transport
100 cannot explain the sea level decline found outside of the wind perturbation region.

101 The subsurface warms substantially around roughly 2/3 of the Antarctic coastline
102 in both models, although at different depth ranges (Fig. 1e,f). In MOM025 intense
103 warming occurs between 200-700 m depth with a maximum warming of > 4°C on the
104 western side of the peninsula after 5 years. This response is roughly equivalent to the
105 previous study wherein a circumpolar wind perturbation was applied in MOM025¹⁷. In
106 MOM01 the warming is focused at shallower depths (75-150 m) with a maximum
107 warming of ~2°C on the western side of the peninsula after 5 years. In both models, the
108 subsurface temperature along the western coastline of the Antarctic Peninsula increases in
109 the first year, with little other evidence of change outside of the perturbation region (Fig.
110 2a; Fig. S2, S3). As the forcing persists, the subsurface warming grows in circumpolar
111 extent and becomes intensified at the peninsula (Fig. 2b; Fig. S2, S3). Yet the near surface
112 ocean temperature west of the Antarctic Peninsula shows little change (cooling of <-
113 0.1°C; Fig. 1d) and the sea ice thickness is slightly increased (2-5 cm, not shown). There
114 is little subsurface temperature change in the Ross Sea sector in both models (Fig. S2, S3).

115 The progressive warming of shelf waters on the western side of the peninsula
116 coincides with a shallowing of isotherms. In the unperturbed state of MOM01 the 0°C
117 isotherm is located at ~125m depth on the western shelf of the peninsula and it shoals by
118 as much as 60m after 5 years of the East Antarctic wind forcing (Fig. 2c,d). In MOM025
119 this isotherm is normally found at ~300m depth and it shoals by as much as 200m with the
120 wind perturbation. The drop in coastal sea level is accompanied by geostrophically-
121 balanced along-shelf coastal velocity anomalies directed north-eastward on the western
122 side of the peninsula and southward on the eastern side (Fig. 2e). As the wind perturbation
123 persists, the sea level and velocity anomalies also progressively increase. After about 3
124 years warming develops on the northeastern coastline of the peninsula (Fig. 2b) primarily
125 from heat being advected eastward around the tip of the peninsula. Upward vertical
126 velocity anomalies on the peninsula shelf (Fig. 2f) are roughly equivalent to the previous
127 study wherein a circumpolar wind perturbation was applied.

128

129 **Mechanisms for intensified subsurface warming**

130 We now examine the physical mechanisms by which East Antarctic wind
131 perturbations can impact Antarctic coastal ocean properties thousands of kilometres away.
132 We begin by tracking the westward coastal propagation of anomalies from their East
133 Antarctic source region to the Ross Sea along a coastal contour that follows the subsurface
134 temperature anomalies on the continental shelf (Fig. 3a). A Hovmöller (distance-time) plot
135 of temperature anomalies at 5-day intervals shows widespread subsurface coastal ocean
136 warming along this contour line and averaged between 200-700m depth in MOM025 and
137 75-150m depth in MOM01 (Fig. 3b,c). The warming develops a focused intensity on the
138 western side of the Antarctic Peninsula, 6000 km away from the western edge of the wind
139 perturbation. In both models subsurface warming on the western side of the peninsula

140 often exceeds 2°C within 5 years.

141 Ensembles of both the unperturbed and wind anomaly simulations reveal the
142 perturbation response relative to background oceanic variability (Methods). In both
143 models, the first indications of change outside of the perturbation region are found
144 scattered on the western side of the peninsula within the first week (not shown). A
145 coherent warming ($<0.1^{\circ}\text{C}$) signature appears on the Hovmöller section near the tip of the
146 peninsula within 50 days (Fig. 3d). After 90 days the Antarctic Peninsula anomaly can
147 locally exceed 0.5°C in both models. When averaged along a section on the western side
148 of the peninsula, the ensemble mean warming at the end of the first year exceeds one
149 standard deviation of the control experiment variability by $+0.14^{\circ}\text{C}$ in MOM01 (Fig. 3e)
150 and 0.3°C in MOM025 (not shown). It takes just 120 days for the ensemble mean
151 warming along this section to exceed one standard deviation of the background oceanic
152 variability in both models.

153 We now describe the physical mechanisms controlling the adjustment of the coastal
154 circulation to the East Antarctic wind perturbation, and explain why the subsurface
155 warming is most intense on the western side of the Antarctic Peninsula. The advective
156 time-scale from the perturbation region via westward coastal currents is more than two
157 years and passive tracers released in the perturbation region never travel around the
158 peninsula. Coastal baroclinic waves (i.e. waves with structure that varies with depth)
159 initiated by wind forcing are capable of remotely modifying the subsurface coastal density
160 structure on faster timescales^{22,23,24}. However, there are several strands of evidence
161 suggesting that baroclinic waves do not make a significant contribution west of the
162 peninsula: i) They are not resolved near Antarctica in MOM025 and are only partially
163 resolved in MOM01²⁵, even though warming is found in both models; ii) The first
164 baroclinic gravity-wave phase speed near the Antarctic coast is <1.0 m/s, requiring >70

165 days for them to reach the peninsula²⁶. Their influence will likely develop gradually,
166 taking longer than the warming time-scale identified in the simulations; iii) Baroclinic
167 waves may have difficulty navigating the complex coastline without substantial
168 dissipation given their small deformation radius²⁷.

169 Westward propagating barotropic coastal Kelvin waves, in contrast, are well resolved
170 by both models. These fast waves carry sea surface height (i.e. sea level) and barotropic
171 (i.e. uniform with depth) current anomalies along the coast, but decay away from the coast
172 over the barotropic deformation radius of $\sim 1000\text{km}$. They can be generated by
173 atmospheric forcing and are observed circumnavigating Antarctica in less than 2 days,
174 with phase speeds of $156\text{-}192\text{ m/s}$ ²⁸. The sea level signature of barotropic waves is clearly
175 identifiable in the simulations with phase speeds that match the theoretical and observed
176 estimates (Fig. 3f). These barotropic Kelvin waves rapidly transmit anomalies westward,
177 driving a progressive drop in coastal sea level away from the perturbation region.

178 To understand the mechanisms by which sea surface height anomalies associated with
179 the barotropic waves modify the subsurface, we now examine an area averaged transect
180 oriented perpendicular to the continental shelf edge on the western side of the peninsula
181 (Fig. 4a). The Southern Ocean State Estimate²⁹ (SOSE) and summer time hydrographic
182 observations^{30,31} suggest that below 100m depth the shelf water temperature in this region
183 ranges from roughly -0.5°C to 1°C , and the vertical and cross-shelf density gradients are
184 weak (Fig. 4b, Fig. S4). In the unperturbed state of MOM025 the shelf water temperature
185 below 100m is often colder than -1°C and there are overly strong cross-shelf and vertical
186 density gradients (Fig. 4c) compared to observations in this region. In the unperturbed
187 state of MOM01, the shelf waters are warmer ($\sim 0.5^\circ\text{C}$) and the density gradients are
188 slightly weaker than observations suggest (Fig. 4d). The two model experiments thus span
189 the observations and the state estimate in this regard, and thereby provide something of an

190 upper and lower bound to the warming that can be attributed to the remote winds. The
191 colder water and stronger density gradients at depth on the shelf lead to a relatively
192 stronger adjustment and warming response at depth in MOM025 compared to that of
193 MOM01.

194 The decrease in sea level around the coastline is mirrored by a lifting of the
195 boundary between the cold near surface water, and the warmer layer below (Fig. 2d,e, Fig.
196 4e,f,g,h). This lifting occurs due to baroclinic adjustment mechanisms occurring both near
197 the seafloor and in the ocean interior on the continental shelf. In MOM025, the main
198 adjustment to the anomalous northeastward barotropic flow develops along the continental
199 shelf edge (Fig. 4e,g,i). The anomalous velocity signal near the shelf edge decreases
200 towards the seafloor (Fig. 4i below 250m), suggesting that bottom friction is acting. This
201 decreased velocity anomaly then allows the anomalous onshore barotropic pressure
202 gradient associated with the cross-shelf sea level gradient anomaly to overcome the
203 anomalous Coriolis force, breaking the constraint of geostrophy, and driving an
204 anomalous up-slope bottom Ekman flow. The upslope flow drives a bottom intensified
205 shallowing of bottom density surfaces and an accompanying subsurface warming (Fig.
206 4e). This warming also penetrates into the interior to influence a layer much thicker than
207 the relatively thin (<30m) Ekman layer through upward diffusion and interior baroclinic
208 adjustment processes^{32,33}.

209 The stronger temperature gradients near the shelf break make this near-bottom
210 isotherm shoaling mechanism more important in MOM025 than MOM01. A similar
211 mechanism is acting in MOM01, however, it occurs closer to the coast where the density
212 and temperature gradients are larger (Fig. 4f,h,j). The maximum temperature change
213 occurs where the temperature gradients, including both vertical and horizontal
214 components, are largest. For both models and the observations, these temperature

215 gradients are largest near the 0°C isotherm on the western side of the peninsula. The
216 warming is deeper in MOM025 since the 0°C isotherm sits deeper on the shelf break and
217 is more sloped than in MOM01. Hydrographic observations may clarify the depth where
218 the maximum temperature response occurs in nature. On an observed cruise line the 0°C
219 isotherm sits on the peninsula shelf break at ~200m depth in the summertime
220 hydrography³¹ (Fig. 4a,b) and it likely deepens in winter. Along the same line the annual
221 mean 0°C isotherm sits on the shelf break at ~400m in MOM025, and ~125m in MOM01
222 (Fig. 4b,c,d); further evidence that the two models provide upper and lower limits to the
223 observed thermal structure.

224 Both bottom and interior processes act in tandem to bring about the necessary
225 adjustment to the barotropic wave anomaly and create warming focused around the 0°C
226 isotherm. While the temperature anomaly in MOM01 appears to be above the seafloor
227 (Fig. 4f), much of it is near the seafloor (Fig. S5) as the bathymetry varies considerably
228 along the Fig.4 section. Overall, these mechanisms facilitate a change of both the
229 barotropic and baroclinic structure of the continental shelf and coastal currents without a
230 local change in wind forcing. The same features are found in other remote locations along
231 the Antarctic coastline. For example, in MOM01 there is a >0.5°C warming in some parts
232 of the Amundsen Sea and the Bellingshausen Sea within five years (Fig. 1, Fig. 2).

233 We conclude that the warming is largest on the western side of the Antarctic Peninsula
234 region for two main reasons. Firstly, the interior temperature gradients are large on the
235 western side of the peninsula due to the close proximity to warm, salty water advected
236 close to the continental shelf by the Antarctic Circumpolar Current (Fig. 4b,c,d, Fig. S4).
237 The presence of this warm, salty Circumpolar Deep Water allows the anomalous flow to
238 create a stronger warming signal in this region. Secondly, we suggest that the anomalous
239 cross-shelf sea level gradients and velocity anomalies are large there due, at least in part,

240 to topographic steering by the particularly steep shelf edge bathymetry (Fig. S6). The
241 depth integrated geostrophic velocity is constrained to follow contours of constant f/h ,
242 where f is the Coriolis parameter and h is the water depth. Consequently, the along-shelf
243 velocity anomalies are strongest along regions of the Antarctic coastline, including the
244 western side of the Antarctic Peninsula, that are characterized by a steep continental slope
245 (Fig. S6a). This region is well connected to the East Antarctic wind perturbation region
246 via f/h contours and the barotropic circulation there responds to changes in winds around
247 the entire Antarctic coastline³⁴. The time-scale and spatial distribution of the velocity
248 created by the East Antarctic wind perturbation is well reproduced in a single-layer
249 shallow-water model, which predicts a particularly strong anomalous barotropic flow
250 along the shelf and shelf break on the western side of the peninsula (Methods, Fig. S6d).
251 The mechanism proposed here predicts the largest onshore transport in regions with the
252 largest alongshore barotropic velocity anomaly.

253

254 **Summary**

255 Figure 5 presents a schematic that summarizes the physical mechanisms whereby
256 barotropic waves forced by a remote Antarctic coastal wind perturbation can rapidly
257 produce intense warming of the subsurface Antarctic coastal ocean with a focused
258 intensity on the western side of the Antarctic Peninsula (Fig. 5). First, a reduction in polar
259 easterlies gradually decreases the local East Antarctic coastal sea level as anomalous
260 surface Ekman transport pumps water offshore. This drop in sea level is then propagated
261 around the Antarctic coastline by a barotropic Kelvin wave. Next, the sea level drop
262 creates a cross-shelf sea level gradient anomaly and an along-shelf geostrophically
263 balanced horizontal velocity anomaly, which is particularly strong on the western side of
264 the Peninsula. Due to both bottom-boundary layer friction and interior adjustment, this

265 horizontal velocity anomaly decreases in the warm, less stratified waters below the
266 thermocline. To maintain geostrophic balance, this anomalous vertical shear is
267 accompanied by a shoaling of the subsurface density layers close to the coast. This
268 shoaling then facilitates the movement of warmer deep water upward onto the continental
269 shelf and toward the coast.

270 A reduction in surface Ekman pumping by a local coastal wind perturbation also
271 creates warming on the shelf¹⁷, as found in the East Antarctic perturbation region in this
272 study. However, here we show that the influence of remote winds on the subsurface
273 coastal ocean can be just as large as that of the local winds. The observed subsurface
274 warming rates on the western side of the peninsula, and in the Amundsen and
275 Bellingshausen Seas are estimated at $\sim 0.5^{\circ}\text{C}$ since 1990⁷. The remote wind perturbation
276 response presented here can create this magnitude of warming in less than a decade. The
277 remote wind perturbation considered here was motivated by the projected influence of the
278 SAM on East Antarctic coastal winds. However, Antarctic coastal wind disturbances are
279 not unique to the SAM or East Antarctica. Well documented links between other climate
280 modes of variability and Antarctic coastal winds can produce a similar barotropic coastal
281 ocean response^{26,35,36}.

282 Accurately modelling observed features of the Antarctic coastal environment
283 requires very fine resolution models. In particular, the inclusion of katabatic winds³⁷, ice
284 cavity interactions^{38,39}, tides²⁰ and mesoscale ocean eddies^{18,19} in the Antarctic coastal
285 region requires horizontal grids finer than 1 km. Eddy driven processes^{18,19} and tidal
286 influences²⁰ certainly play a role in the equilibrium heat budget on the continental shelf,
287 but it is difficult to predict significant changes to them. At finer resolution a more
288 vigorous mesoscale eddy field could further enhance cross-shelf exchange of warm water.
289 Observations also suggest that Antarctic Circumpolar Current filaments impinging on the

290 shelf break can generate onshore flows in topographic channels via bottom Ekman
291 dynamics similar to those presented here⁴⁰. Remotely generated sea level anomalies may
292 drive a portion of these topographic channel intrusions. Currently there is no theoretical
293 framework or numerical model that can simultaneously represent all the relevant
294 processes, making quantitative comparisons between the relevant mechanisms difficult.

295 We have documented the sensitivity of the Antarctic coastal ocean to remote
296 atmospheric wind perturbations, particularly ocean properties on the western side of the
297 Antarctic Peninsula. This sensitivity is due to a conspiracy between the proximity of the
298 relatively warm Circumpolar Deep Water and the steep shelf bathymetry in the region,
299 with circumpolar impacts facilitated by coastal-trapped barotropic waves. This
300 mechanism helps explain the vulnerability of the West Antarctic marine grounded ice
301 sheets to subsurface ocean warming, with potentially profound implications for global sea
302 level rise over the coming decades.

303

304 **References**

- 305 1. Hay, C., Morrow, E., Kopp, R., and Mitrovica, J. Probabilistic reanalysis of
306 twentieth-century sea-level rise, *Nature*, 517 (7535), 481, (2015).
- 307 2. Hock, R., de Woul, M., Radic, V., and Dyurgerov, M. Mountain glaciers and ice
308 caps around Antarctica make a large sea-level rise contribution. *Geophys. Res.*
309 *Lett.*, 36, L07501, (2009).
- 310 3. Harig, C., and Simon, F. Accelerated West Antarctic ice mass loss continues to
311 outpace Antarctic gains, *Earth and Planetary Science Letters*, 415, 134-141,
312 (2015).

- 313 4. Li, X., Rignot, E., Morlighem, M., Mouginot, J., Scheuchl, B. Grounding line
314 retreat of Totten Glacier East Antarctica. 1996-2013, *Geophys. Res. Lett.*, 42,
315 8049-8056, (2015).
- 316 5. Rignot, E., and Jacobs, S. Rapid bottom melting widespread near Antarctic ice
317 sheet grounding lines. *Science*, 296, 2020–2023, (2002).
- 318 6. Rignot, E., Jacobs, S., Mouginot, J., and Scheule, B. Ice-Shelf Melting around
319 Antarctica, *Science*, 341, 266-270, (2013).
- 320 7. Schmidtko, S., Heywood, K., Thompson, A., Aoki, S. Multidecadal warming of
321 Antarctic waters, *Science*, 346, 1227-1231, (2014).
- 322 8. Sea Level Change – Chapter 13 of IPCC Working Group 1 Fifth Assessment
323 Report. editors Church, J. A. et al., [https://www.ipcc.ch/pdf/assessment-](https://www.ipcc.ch/pdf/assessment-report/ar5/wg1/WG1AR5_Chapter13_FINAL.pdf)
324 [report/ar5/wg1/WG1AR5_Chapter13_FINAL.pdf](https://www.ipcc.ch/pdf/assessment-report/ar5/wg1/WG1AR5_Chapter13_FINAL.pdf), (2013).
- 325 9. Joughin, I., Smith, B. E., and Medley, B. Marine ice sheet collapse potentially
326 under way for the Thwaites Glacier Basin. West Antarctica. *Science*, 344(6185),
327 735-738, (2014).
- 328 10. Favier, L., et al. Retreat of Pine Island Glacier controlled by marine ice-sheet
329 instability. *Nature Climate Change*, 4(2), 117-121, (2014).
- 330 11. DeConto, R., and Pollard, D. Contribution of Antarctica to past and future sea-
331 level rise. *Nature*, 531, 591-597, (2016).
- 332 12. Jacobs, S. S. On the nature and significance of the Antarctic Slope Front, *Mar.*
333 *Chem.*, **35**, 9–24, doi:10.1016/S0304-4203(09)90005-6 (1991).
- 334 13. Rignot, E., et al. Recent Antarctic ice mass loss from radar interferometry and
335 regional climate modeling. *Nat. Geosci.*, 1, 106–110, (2008).
- 336 14. Cook, A., et al. Ocean forcing of glacier retreat in the western Antarctic Peninsula.
337 *Science*, 353, 283-285 (2016).

- 338 15. Thompson, D. W., and Solomon, S. Interpretation of recent Southern Hemisphere
339 climate change. *Science*, 296, 895-899, (2002).
- 340 16. Martinson, D., Stammerjohn, S., Iannuzzi, R., Smith, R., and Vernet, M. Western
341 Antarctic Peninsula physical oceanography and spatio-temporal variability. *Deep*
342 *Sea Res. Part II*, 55, 1964-1987, (2008).
- 343 17. Spence, P., et al. Rapid subsurface warming and circulation changes of Antarctic
344 coastal waters by poleward shifting winds, *Geophys. Res. Lett.*, 41 (13), 4601-
345 4610, (2014).
- 346 18. Nøst, O. A., et al. Eddy overturning of the Antarctic Slope Front controls glacial
347 melting in the Eastern Weddell Sea. *J. Geophys. Res.*, 116, C11014,
348 doi:10.1029/2011JC006965, (2011).
- 349 19. Stewart, A., and Thompson, A. Connecting Antarctic cross-slope exchange with
350 Southern Ocean overturning, *J. Phys. Oceanogr.*, 43, 1453–1471, (2013).
- 351 20. Flexas, M. et al., Role of tides on the formation of the Antarctic Slope Front at the
352 Weddell-Scotia Confluence, *J. Geophys. Res. Oceans*, 120, 3658–3680, (2015).
- 353 21. Zheng, F., Li, J., Clark, R., and Nnamchi, H. Simulation and projection of the
354 Southern Hemisphere Annular Mode in CMIP5 models. *J. Clim.*, 26, 9860–9879,
355 (2013).
- 356 22. Rhines, P.B. Edge-, Bottom-, and Rossby Waves in a Rotating Stratified Fluid,
357 *Geophys. Fluid Dyn.*, 1, 273-302, (1970).
- 358 23. Rhines, P and Bretherton, F. Topographic Rossby waves in a rough-bottomed
359 ocean. *J. Fluid Mech.*, 61 (3), 583-607, (1973).
- 360 24. Wang, D., and Mooers, C. Coastal-Trapped Waves in a Continuously Stratified
361 Ocean, *J. Phys. Oceanogr.*, 6, 1976, (1976).

- 362 25. Hallberg, R. Using a resolution function to regulate parameterizations of oceanic
363 mesoscale eddy effects, *Ocean Modell.*, 72, 92-103, (2013).
- 364 26. Chelton, D., et al. Geographical variability of the first baroclinic Rossby radius of
365 deformation. *J. Phys. Oceanogr.*, 28, 433-460, (1998).
- 366 27. Schwab, D. J., and Beletsky, D. Propagation of Kelvin waves along irregular
367 coastlines in finite-difference models. *Advances in water resources*, 22.3, 239-245,
368 (1998).
- 369 28. Kushara, K., and Ohshima, K. Kelvin Waves around Antarctica. *J. Phys.*
370 *Oceanogr.*, 44, 2909-2920, (2014).
- 371 29. Mazloff, M. R., Heimbach, P., and Wunsch, C. An eddy-permitting Southern
372 Ocean state estimate. *J. Phys. Oceanogr.*, 40, 880–899, (2010).
- 373 30. Moffat, C., Owens, B, and Beardsley, R. On the characteristics of Circumpolar
374 Deep Water intrusions to the west Antarctic Peninsula shelf. *J. Geophys. Res.*, 114,
375 C05017, (2009).
- 376 31. Chipman D. W., et al. Carbon Dioxide, Hydrographic, and Chemical Data
377 Obtained During the R/V Akademik Ioffe Cruise in the South Pacific Ocean
378 (WOCE Section SO4P, February-April 1992). ORNL/CDIAC-100, NDP-063.
379 Carbon Dioxide Information Analysis Center, Oak Ridge National Laboratory,
380 U.S. Department of Energy, Oak Ridge, Tennessee. doi:
381 10.3334/CDIAC/otg.ndp063
- 382 32. MacCready, P., and P. B. Rhines. Buoyant inhibition of Ekman transport on a
383 slope and its effect on stratified spin-up. *J. Fluid Mech.*, 223, 631–666, (1991).
- 384 33. Wåhlin, A. et al. Some Implications of Ekman Layer Dynamics for Cross-Shelf
385 Exchange in the Amundsen Sea. *J. Phys. Oceanogr.*, 42, 1461–1474, (2012).

- 386 34. Hughes et al. Wind-Driven Transport Fluctuations through Drake Passage: A
387 Southern Mode. *J. Phys. Ocean.*, 29, 1971-1992, (1999).
- 388 35. Karoly, D. J. Southern hemisphere circulation features associated with El Niño-
389 Southern Oscillation events. *J. Clim.* 2, 1239–1252, (1989).
- 390 36. Jenkins et al. Decadal Ocean Forcing and Antarctic Ice Sheet Response: Lessons
391 from the Amundsen Sea. *Oceanography*, 29(4), 106-117.
- 392 37. Mathiot, P., et al. Sensitivity of Coastal Polynyas and High Salinity Shelf water
393 Production in the Ross Sea, Antarctica, to the Atmospheric Forcing. *Ocean*
394 *Dynam.*, 62, 701-723, (2012).
- 395 38. Dinniman, S., Klinck, J., and Smith, W. A model study of Circumpolar Deep
396 Water on the West Antarctic Peninsula and Ross Sea continental shelves. *Deep Sea*
397 *Res., Part II*, 58, 1508–1523, (2011).
- 398 39. Hellmer, H. H., Kauker, F., Timmermann, R., Determann, J., and Rae, J. Twenty-
399 first-century warming of a large Antarctic ice-shelf cavity by a redirected coastal
400 current. *Nature*, 485, 225-228, (2012).
- 401 40. Wåhlin, A.K. et al. Some Implications of Ekman Layer Dynamics for Cross-Shelf
402 Exchange in the Amundsen Sea. *J. Phys. Oceanogr.*, 42, 1461–1474, (2012)

403

404

405 Please send correspondence to paul.spence@unsw.edu.au

406

407 **Acknowledgements**

408 This research was undertaken on the National Computational Infrastructure (NCI) in
409 Canberra, Australia, which is supported by the Australian Commonwealth Government.

410 Thanks to Stuart Ramsden and the NCI Vizlab for helping with the schematic in Fig. 5.

411 Thanks to NOAA/GFDL for helping with model developments. Thanks to Nicolas
412 Jourdain for providing Fig. S1 and helpful comments. Thanks to Elisa Bergkamp for
413 investigating baroclinic modes in idealized simulations and to Oleg Saenko, Julien Le
414 Sommer, Andrew Stewart, Jeremy Fyke, Robert Hallberg, Carolina Dufour,
415 Gustavo Marques and Paul Goddard for helpful comments. PS was supported by an
416 Australian Research Council (ARC) DECRA Fellowship DE150100223, AMH by an
417 ARC Future Fellowship FT120100842 and MHE by an ARC Laureate Fellowship
418 FL100100214.

419

420 **Author Contributions**

421 P.S. conceived the study, conducted the global ocean modelling and wrote the initial draft
422 of the paper. R.M.H. did the single layer, shallow-water modelling. P.S. and R.M.H.
423 analysed the model data. All authors contributed to interpreting the results, discussion of
424 the associated dynamics, and refinement of the paper.

425

426 **Competing Financial Interests Statement**

427 The authors declare no competing financial interests.

428

429 **Methods**

430 **The Global Ocean-Sea ice Model**

431 This study primarily uses two global ocean, sea-ice models referred to as MOM025
432 and MOM01 that differ only in the resolution of their vertical and horizontal grids.
433 MOM025 is the same model configuration as used in Spence et al. [2014]¹⁷ and has a $1/4^\circ$
434 Mercator horizontal resolution with ~ 11 km grid spacing at 65°S and 50 vertical levels.
435 MOM01 has a $1/10^\circ$ Mercator horizontal resolution with ~ 4.5 km grid spacing at 65°S and

436 75 vertical levels. The Antarctic Slope Front and Antarctic coastal currents have observed
437 horizontal widths of ~50 km, except in regions of particularly steep bathymetry (e.g. Ross
438 Sea) where the observed horizontal scale is reduced to ~20km^{12,41,42}. Sea surface salinity is
439 restored to seasonally varying climatology on a 60-day time-scale with a piston velocity of
440 0.16 m/day. The atmospheric state is prescribed and converted to ocean surface fluxes by
441 bulk formulae, consequently the model does not resolve air-sea feedbacks. The
442 atmospheric forcing is derived from version 2 of the Coordinated Ocean-ice Reference
443 Experiments Normal Year Forcing (CORE-NYF) reanalysis data⁴³. CORE-NYF provides
444 a climatological mean atmospheric state estimate at 6-hour intervals and roughly 2-degree
445 horizontal resolution, along with representative synoptic variability. The 1/4° and 1/10°
446 models are based on the GFDL CM2.5 and GFDL CM2.6 coupled climate models^{44,45}
447 respectively.

448 The models do not have ice shelf cavities and their horizontal resolution is insufficient
449 to adequately resolve the first baroclinic Rossby radius of deformation on the Antarctic
450 continental shelf, which requires horizontal grids finer than 1/36° Mercator resolution (< 1
451 km)²⁵. However, comparisons between the MOM01 and MOM25 simulations allow an
452 understanding of the sensitivity of the results to the presence of a more vigorous eddy-
453 field as the horizontal grid is refined from 1/4° to 1/10° Mercator resolution and the
454 vertical resolution is increased from 50 to 75 vertical levels. In particular, we note that
455 increasing the vertical resolution greatly enhances the barotropic and baroclinic eddy
456 kinetic energies on and surrounding the Antarctic continental shelf and slope⁴⁶.

457

458 **Control State Simulations**

459 Idealized Antarctic coastal wind perturbation experiments are initiated in the 1/4°
460 and 1/10° models from 200-year and 50-year long control state simulations that are forced

461 by repeated CORE-NYF atmospheric state. The control state water mass properties are
462 evaluated on the western side of the peninsula by comparing to the 1/6° Mercator
463 resolution and 46 vertical level Southern Ocean State Estimate (SOSE)²⁹ and the World
464 Ocean Circulation Experiment (WOCE) line SO4P of hydrographic observations³¹. For
465 the SOSE comparison across-shelf-depth slices averaged along a large portion of the
466 peninsula are used (Fig. 4). The continental shelf waters in this section are >1°C colder in
467 MOM025 and >0.5°C warmer in MOM01 than in SOSE. Similarly, the sloped isopycnals
468 on the continental shelf are steeper in MOM025 and flatter in MOM01 than in SOSE.
469 When averaged between 100m and 500m depth within 50km of the continental shelf edge
470 the across shelf temperature gradient is 0.82 °C / 100 km in SOSE, 2.80 °C / 100 km in
471 MOM025 and 0.68°C / 100 km in MOM01. When evaluated along the WOCE SO4P line,
472 the models exhibit similar temperature biases (Fig. S4). The continental shelf waters are
473 often >1°C colder in MOM025 and >0.5°C warmer in MOM01 than in the WOCE SO4P
474 data. The 0°C isotherm that characterizes the simulated warming response crosses the
475 shelf break on the SO4P line at a depth of ~200m in WOCE, ~100m in SOSE, ~400m in
476 MOM025 and ~125m in MOM01. Hence, the water mass structures in MOM01 and
477 MOM025 straddle the observations, and thus may provide a range for the temperature
478 response.

479

480 **Wind Perturbation Experiments**

481 The primary wind perturbation scenario used in this study is based on the $W_{4^{\circ}S+15\%$
482 $(62^{\circ}S-70^{\circ}S)$ scenario of Spence et al. [2014]¹⁷, wherein the CORE-NYF 10 m winds at all
483 longitudes between 62°S and 70°S are shifted four degrees south and increased in
484 magnitude by 15%. This perturbation scenario was guided by an assessment of the late
485 21st Century change in Southern Ocean zonal winds in 32 climate models from the Fifth

486 Coupled Model Intercomparison Project (CMIP5). The only difference between the
487 $W_{4^{\circ}S+15\% (62^{\circ}S-70^{\circ}S)}$ scenario of Spence et al. [2014]¹⁷ and the experiment considered here is
488 that the wind perturbation is applied exclusively along the East Antarctic coastline
489 between 20°E-120°E (Fig. 1a,b). The wind perturbation scenario is motivated by the
490 Antarctic polar easterly winds and their SAM regression being strongest along the East
491 Antarctic coastline in both the CMIP5 multi-model ensemble and the CORE 1948-2007
492 reanalysis data (Fig. 1a, see also Fig. S1). The wind forcing perturbation is applied as a
493 constant anomaly to the CORE-NYF atmospheric state. Both meridional and zonal wind
494 components are modified and smoothing is applied along the wind perturbation
495 boundaries. Several other Antarctic wind perturbation scenarios were tested, and in all
496 cases the ocean response was robust and roughly a linear function of the wind perturbation
497 scenario. For example, the ocean response takes longer to manifest on the peninsula when
498 the perturbation is ramped over time or applied further eastward, and it is weaker when the
499 wind perturbation area is reduced.

500 All anomalies presented here are determined as the difference between the wind
501 perturbation simulation and the concomitantly extended control simulation, with this
502 approach acting to approximately remove the effects of model drift. The model results
503 were validated with ten-member ensembles of both the control and perturbed experiments
504 to identify the role of internal variability in the perturbation response. The ensembles are
505 not necessary to clearly identify the perturbation response, and thus anomalies are often
506 presented as the difference between a single control and perturbed experiment member.
507 However, at time-scales ≤ 1 year we choose to show an ensemble average anomaly based
508 on daily averages to clarify the wind response. Separately averaging the ten-members of
509 each ensemble, and then taking their difference determines the ensemble average anomaly.
510

511 **Single-Layer Shallow Water Ocean Model Experiments**

512 In order to examine the dynamics of barotropic coastally-trapped waves, a single-
513 layer ocean simulation was considered with similar forcing as the localized wind
514 perturbation experiment considered here. For this purpose, we used the Regional Ocean
515 Modelling System⁴⁷ (ROMS) in a linear, single-layer shallow water configuration with a
516 similar grid and bathymetry to MOM025, yet restricted to the region south of 30°S (where
517 a radiation boundary condition was used). The simulation was initialized from rest, and
518 forced with the temporally constant zonal wind stress anomaly applied in the perturbation
519 simulation of the global ocean sea-ice models (i.e. Fig. 1b) and run for 20 days with
520 quadratic bottom drag.

521

522 **Data Availability**

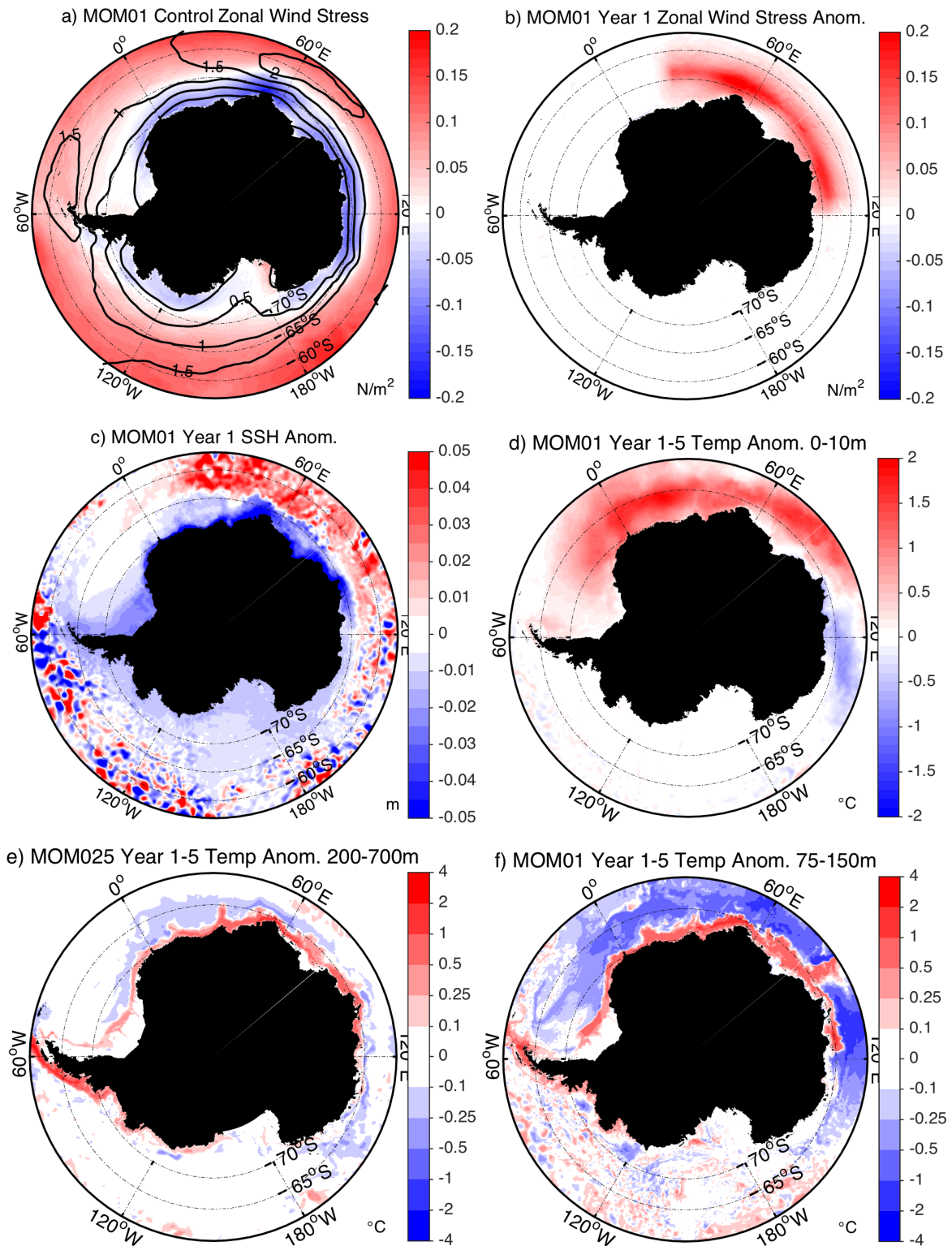
523 The Southern Ocean State Estimate data that supports this study is publicly
524 available at http://sose.ucsd.edu/sose_stateestimation_data_05to10.html. The World
525 Ocean Circulation Experiment line SO4P hydrographic observations are publicly available
526 at <https://www.nodc.noaa.gov/woce/wdiu/>. All MOM025, MOM01 and ROMS model
527 simulation data is available from the corresponding author upon reasonable request.

528

529 **Methods References**

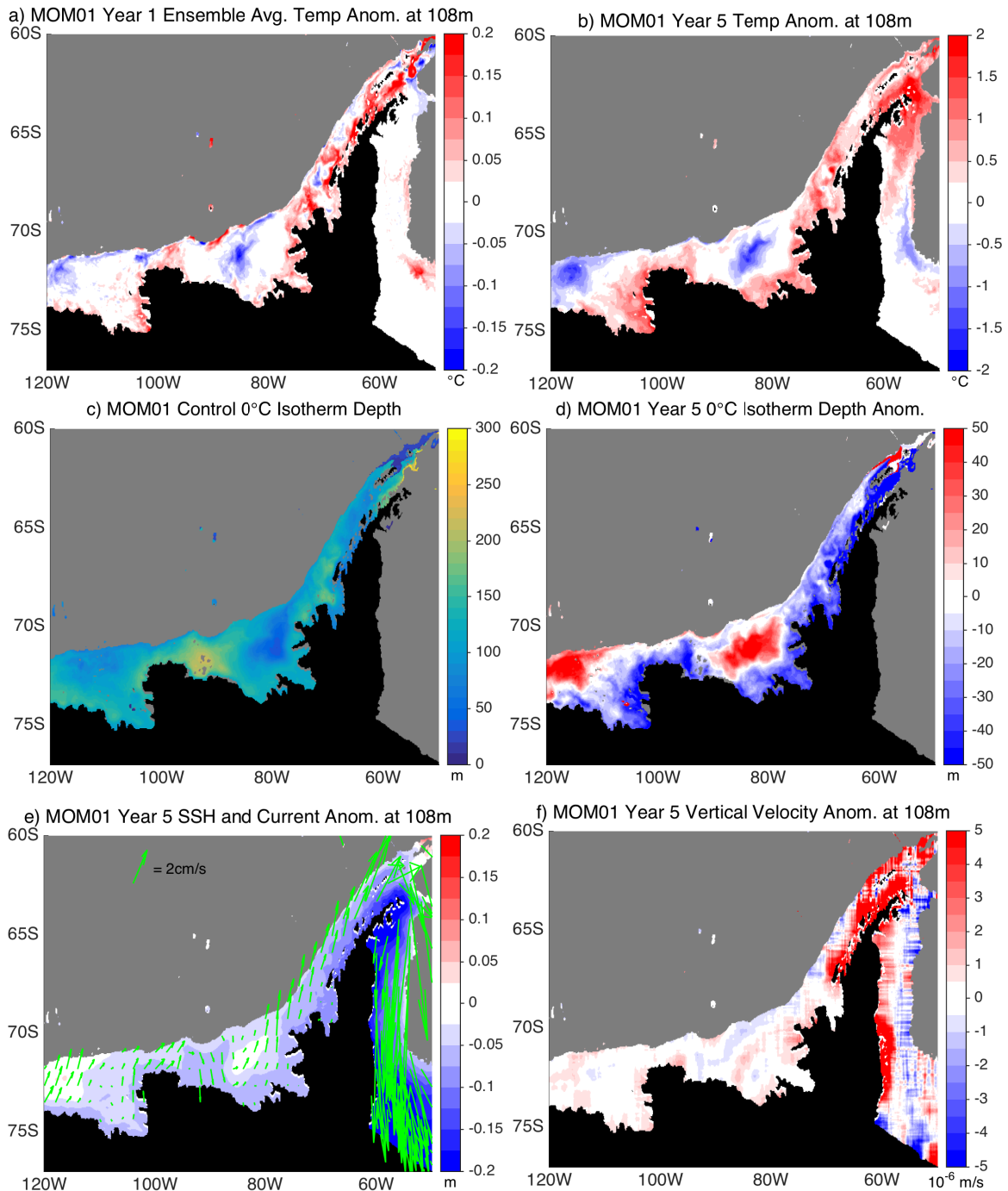
- 530 41. Dong, J., Speer, K., Jullion, L. The Antarctic Slope Current near 30°E, *Geophys.*
531 *Res. Lett.*, 121 (2), 1051-1062, (2016).
- 532 42. Chavanne, C. P., Heywood, K., Nicholls, K., and Fer, I. Observations of the
533 Antarctic Slope Undercurrent in the southeastern Weddell Sea. *Geophys. Res.*
534 *Lett.*, 37, L13601, doi:10.1029/2010GL043603 (2010).

- 535 43. Large, W. G., and Yeager, S. The global climatology of an inter-annually varying
536 air-sea flux data set. *Clim. Dyn.*, 33, 341-364, (2009).
- 537 44. Griffies, S.M., et al. Impacts on ocean heat from transient mesoscale eddies in a
538 hierarchy of climate models. *J.Clim.*, 28, 952-977, (2015).
- 539 45. Delworth, T. L., et al. Simulated climate and climate change in the GFDL CM2.5
540 high-resolution coupled climate model, *J. Clim.*, 25, 2755-2781, (2012).
- 541 46. Stewart, K., et al. Vertical resolution of baroclinic modes in global ocean models,
542 *Ocean Model.*, 113, 50-65, (2017).
- 543 47. Shchepetkin, A., and McWilliams, J. The regional oceanic modeling system
544 (ROMS): a split-explicit, free surface, topography following-coordinate oceanic
545 model. *Ocean Modell.*, 9 (4), 347-401.



546 **Figure 1 | Annual mean model response to East Antarctic poleward intensifying**
 547 **winds.** (a, colors) Annual mean zonal wind stress (N/m^2) in the MOM01 control
 548 simulation. (a, contour lines) Zonal wind speed regression (m/s) on the non-dimensional
 549 SAM index (defined as the index minus its mean divided by its standard deviation, both

550 mean and standard deviation being calculated considering only values prior to 1970). The
551 SAM index is calculated by subtracting the zonal mean sea level pressure at the latitude
552 closest to 65°S from the zonal mean sea level pressure at the latitude closest to 40°S. We
553 use the CORE-II reanalysis sea level pressure and 10m winds over 1948-2007 for the
554 regression³⁷. (b) Annual mean zonal wind stress anomaly (N/m²), (c) sea surface height
555 anomaly (m), and (d) ocean temperature (°C) anomaly averaged between 0-10m depth in
556 year 1 of the MOM01 wind perturbation simulation. Note that panels a-d are essentially
557 the same for the MOM025 model. (e) MOM025 ocean temperature (°C) anomaly
558 averaged between 200-700m depth and years 1 to 5 of the wind perturbation. (f) MOM01
559 ocean temperature (°C) anomaly averaged between 75-150m depth and years 1 to 5 of the
560 wind perturbation. Note the non-linear color scale in panels (e) and (f).
561



563

564

Figure 2 | Antarctic Peninsula shelf response to East Antarctic poleward intensifying

565

winds. (a) MOM01 ensemble mean temperature anomaly (°C) computed as the difference

566

between the ten-member ensemble mean of the perturbation and control simulations over

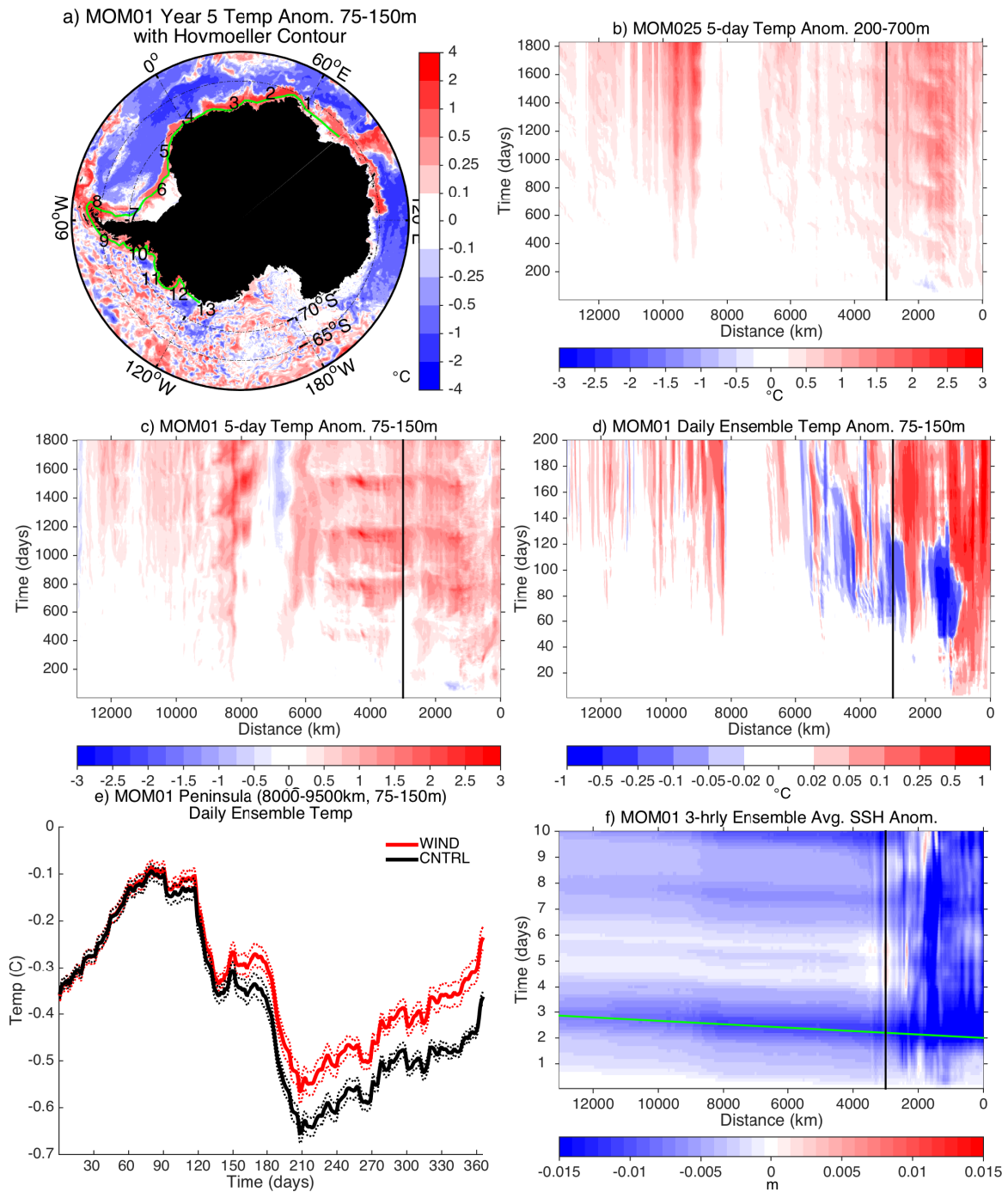
567

the first year at 108 m depth. (b) MOM01 annual mean temperature anomaly (°C) at 108m

568

depth in the fifth year of perturbation. (c) Depth (m) of the 0°C isotherm in the MOM01

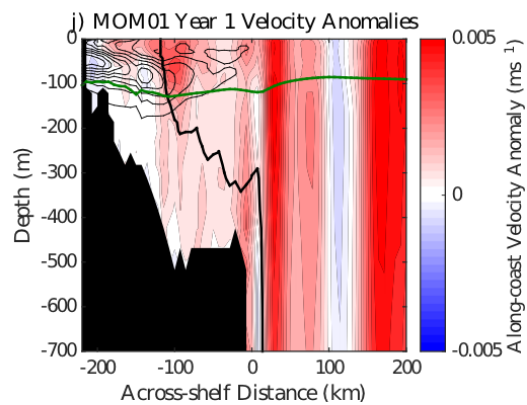
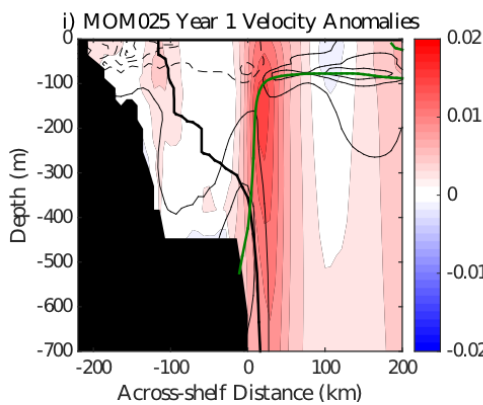
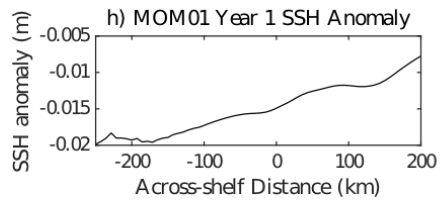
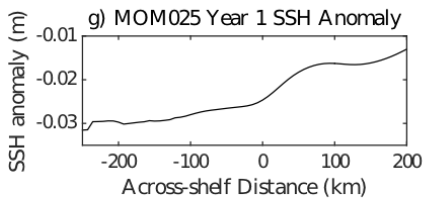
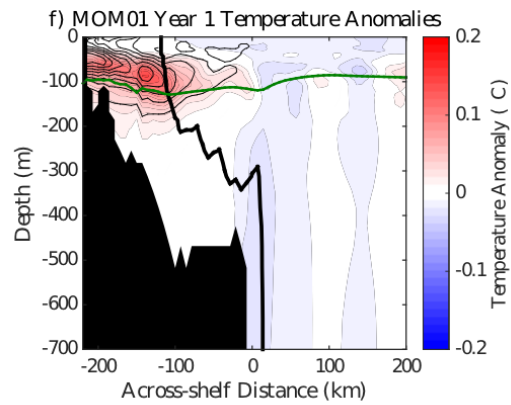
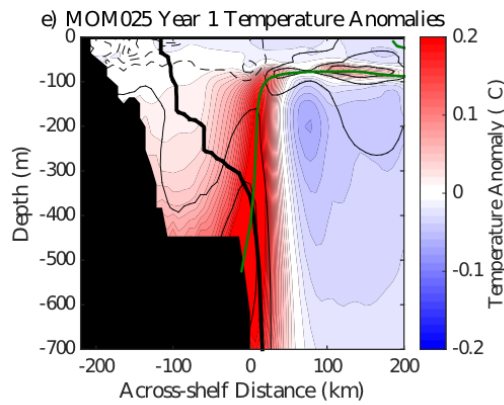
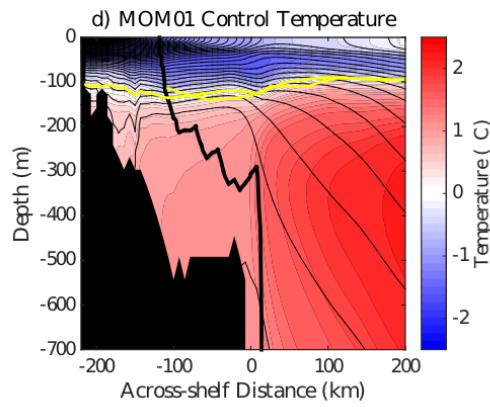
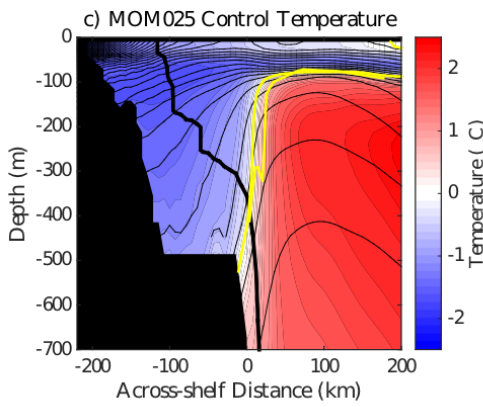
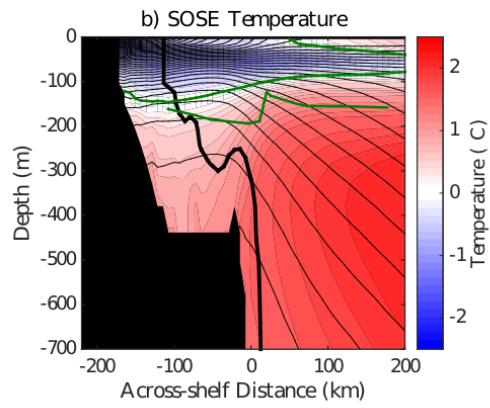
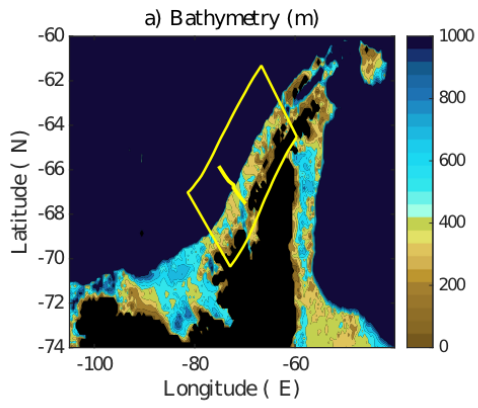
569 control state. (d) MOM01 0°C isotherm depth (m) anomaly in year 5. (e) MOM01 sea
570 surface height (colors, m) anomaly and current anomaly (vectors, cm/s) at 108m depth in
571 year 5 of the perturbation. The current anomaly is area smoothed and every 10th vector is
572 plotted. (f) MOM01 area smoothed vertical velocity (m/s, positive upwards) anomaly in
573 year 5. Note regions with depths >2000m are shaded gray in all panels. In panels c and d
574 gray shading masks both depths >1000m and places where the 0°C isotherm is not found
575 at depths <1000m.



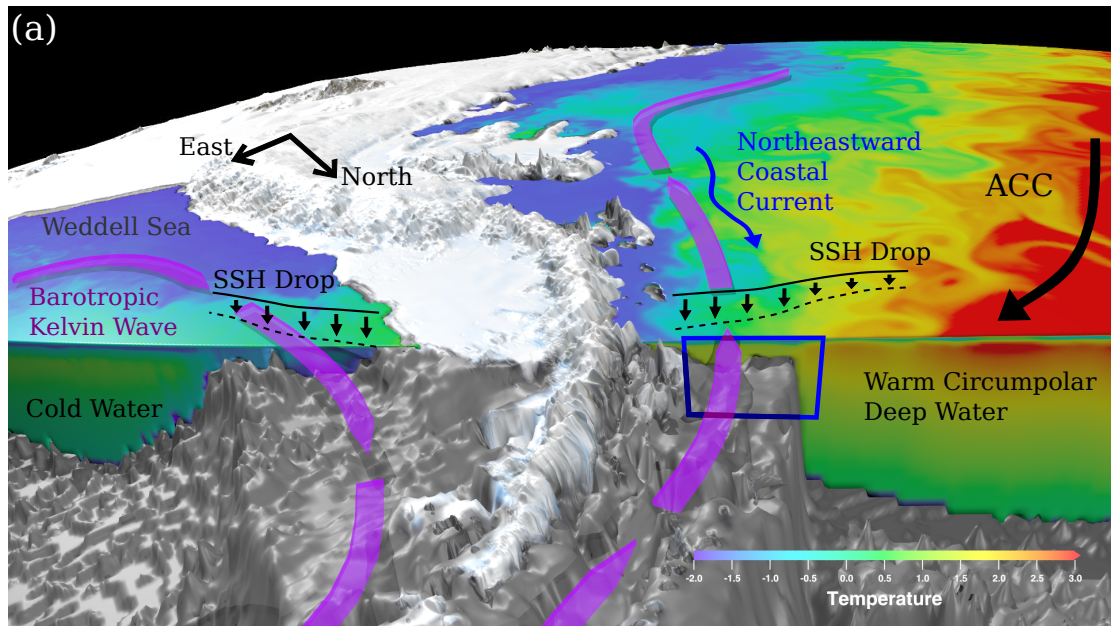
576

577 **Figure 3 | Hovmöller and time-series plots of Antarctic coastal ocean response to**
 578 **East Antarctic poleward intensifying wind forcing.** (a) MOM01 annual mean ocean
 579 temperature (°C) anomaly averaged between 75-150m depth in year 5 of the wind
 580 perturbation. Values in panels (b-f) are averaged over a $\sim 3500 \text{ km}^2$ area around points on
 581 the green coastal contour line in (a). Black numbers along the green line indicate the
 582 distance along the contour in 1000 km intervals. (b) Hovmöller (distance-time) of 5 years

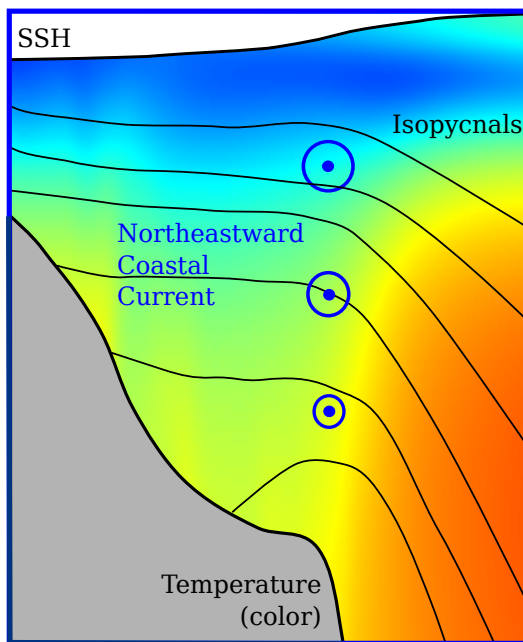
583 of average temperature anomalies ($^{\circ}\text{C}$) between 200-700m depth at 5-day intervals in
584 MOM025. The tip of the Antarctic Peninsula is at $\sim 8200\text{km}$ on the x-axis. (c) Same as (b)
585 except averaged 75-150m depth in MOM01. (d) Hovmöller of daily ensemble mean
586 temperature anomalies ($^{\circ}\text{C}$) computed as the difference between the ten-member ensemble
587 mean of the perturbation and control simulations over the first year averaged between 75-
588 150m depth in MOM01. (e) Ensemble time-series of daily temperature ($^{\circ}\text{C}$) averaged
589 between 75-150m depth and over the 8000-9500km section of the coastal contour in panel
590 (a), which is located on the western side of the West Antarctic Peninsula. The solid red
591 (black) line is the 10-member ensemble mean in wind perturbation (control) simulation.
592 The dashed lines indicate a 1 standard deviation range among the ensemble members. (f)
593 Hovmöller of ensemble mean coastal sea level anomaly (m) at 30-minute intervals for 60
594 days in MOM01. The green line in (f) indicates the theoretical prediction for the phase
595 speed of a barotropic coastal Kelvin wave (roughly $156\text{-}192\text{ m/s}$)²⁶. The vertical black line
596 in panels (b,c,d,f) indicates the western edge of the wind perturbation region.



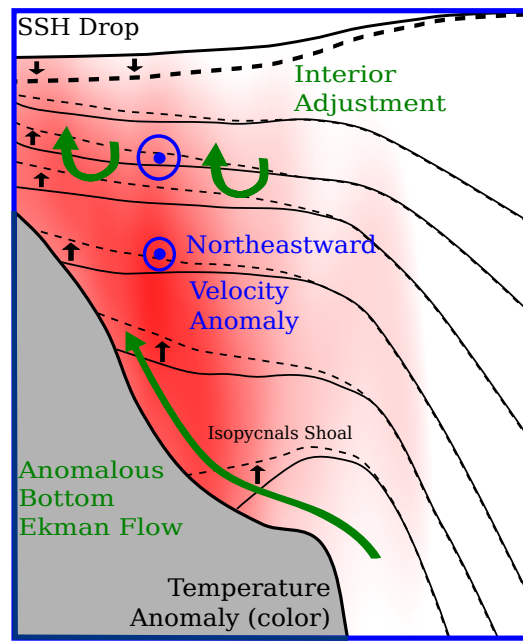
598 **Figure 4 | Across-shelf transects of western side of peninsula response to East**
599 **Antarctic wind perturbation.** (a) Depth of bathymetry (m) on the Antarctic Peninsula.
600 Across-shelf-depth slices in (b-j) are averaged along the shelf within the green region in
601 (a). Yellow markers in (a) indicate the World Ocean Circulation Experiment line SO4P of
602 hydrographic observations. (b) The Southern Ocean State Estimate temperature (color; the
603 green indicates the 0°C isotherm) and 0.1kg/m³ density contours (black) averaged along
604 the shelf within the green box in (a). The yellow line in (b) indicates the 0°C isotherm
605 from hydrographic observation along the SO4P line. (c-d) Same as (b) except for the
606 unperturbed state of MOM025 and MOM01, and the yellow line indicates the 0°C
607 isotherm in the models along the SO4P line. Year 1 ensemble average temperature
608 anomalies for (e) MOM025 and (f) MOM01, with 0.005kg/m³ density anomaly contours
609 (solid = positive, dashed = negative). Year 1 ensemble average along-shelf sea surface
610 height anomaly for (g) MOM025 and (h) MOM01. Year 1 ensemble average along-shelf
611 velocity anomalies for (i) MOM025 and (j) MOM01, with 0.005kg/m³ density anomaly
612 contours. Locations where less than 20% of the grid points along the section at that x-z
613 location were within the ocean have been masked out in black, and the thick black line
614 indicates where 90% of grid points were within the ocean.
615



(b) Control



(c) Anomaly



616

617 **Figure 5 | Schematic of the warming response of West Antarctic Peninsula waters to**

618 **East Antarctic wind perturbation.** (a) View of the West Antarctic Peninsula

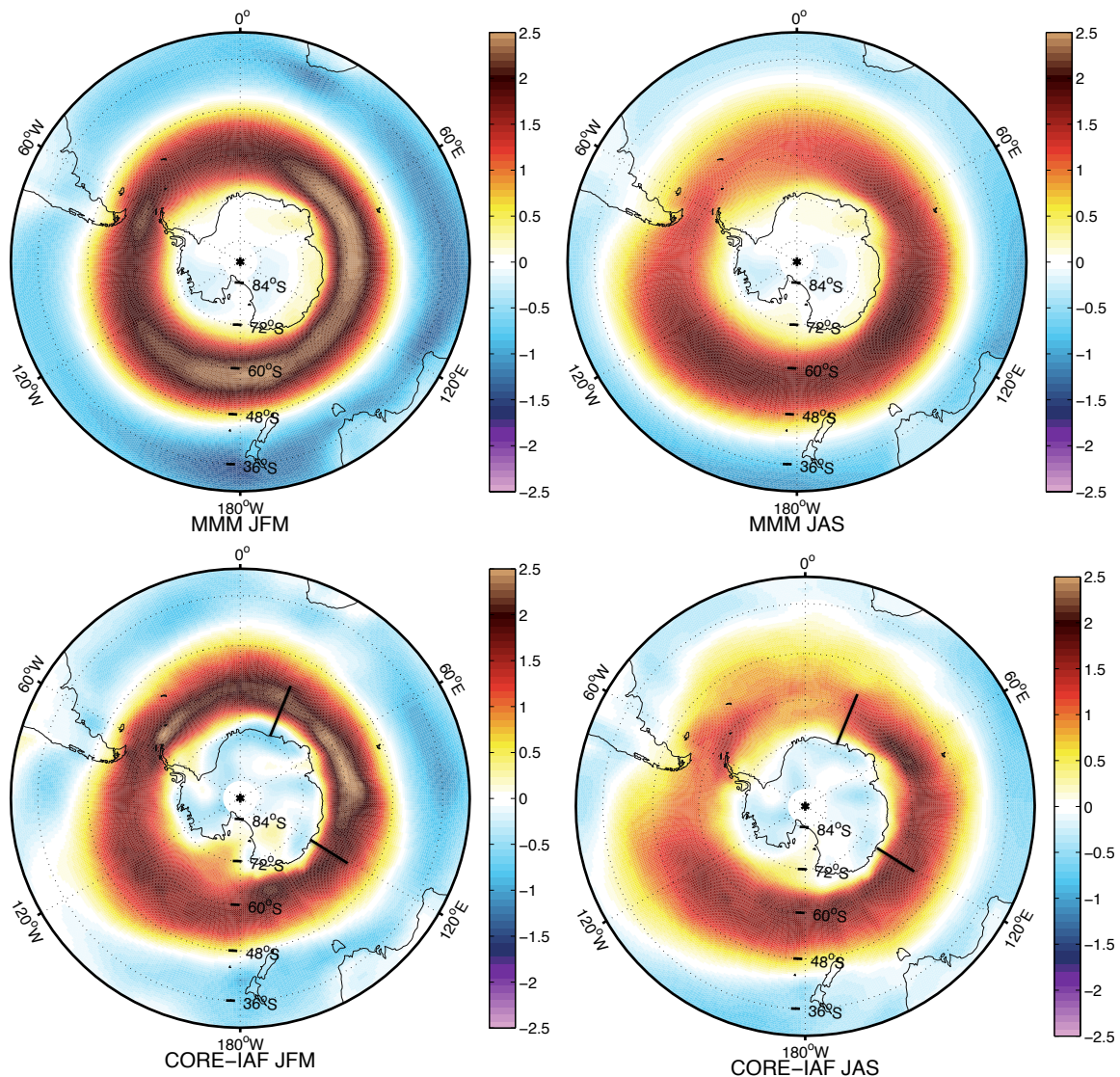
619 with bathymetry in grey shading, and temperature in color. Note the warm Circumpolar

620 Deep Water brought close to the continent by the Antarctic Circumpolar Current (ACC)

621 on the western side. The purple arrows indicate the pathway of barotropic Kelvin waves

622 propagating from East Antarctica. The blue box illustrates the location of across shelf

623 transects in panels (b) and (c). (b) Vertical, across-shelf transect on the western side of the
624 peninsula showing the temperature structure (color) and density surfaces (black isopycnal
625 contours) in an unperturbed state. The low sea surface height near the coast is associated
626 with the geostrophic northeastward coastal current (blue arrow heads indicating flow out
627 of the page and the surrounding circle size indicating the flow strength). (c) Vertical,
628 across-shelf transect on the western side of the peninsula of anomalies initiated by
629 barotropic Kelvin waves generated by an East Antarctic wind perturbation. Barotropic
630 Kelvin waves transmit a drop in coastal sea level along the Antarctic coastline, creating a
631 northeastward barotropic velocity anomaly. In response, the interior isopycnals
632 shoal through both interior baroclinic adjustment and anomalous up-slope bottom Ekman
633 flow (green arrows), allowing the velocity anomaly to decay with depth (blue arrow
634 heads). The shoaling of isopycnals brings warm, deep water upwards and towards the
635 coast driving subsurface warming (color).



636

637 **Supplementary Figure 1 | CORE-II and CMIP5 Multi-Model Mean (MMM) zonal**

638 **wind speed regression on the non-dimensional SAM index.** Zonal wind speed

639 regression on the non-dimensional SAM index (defined as the index minus its mean

640 divided by its standard deviation, both mean and standard deviation being calculated

641 considering only values prior to 1970). The SAM index is calculated by subtracting the

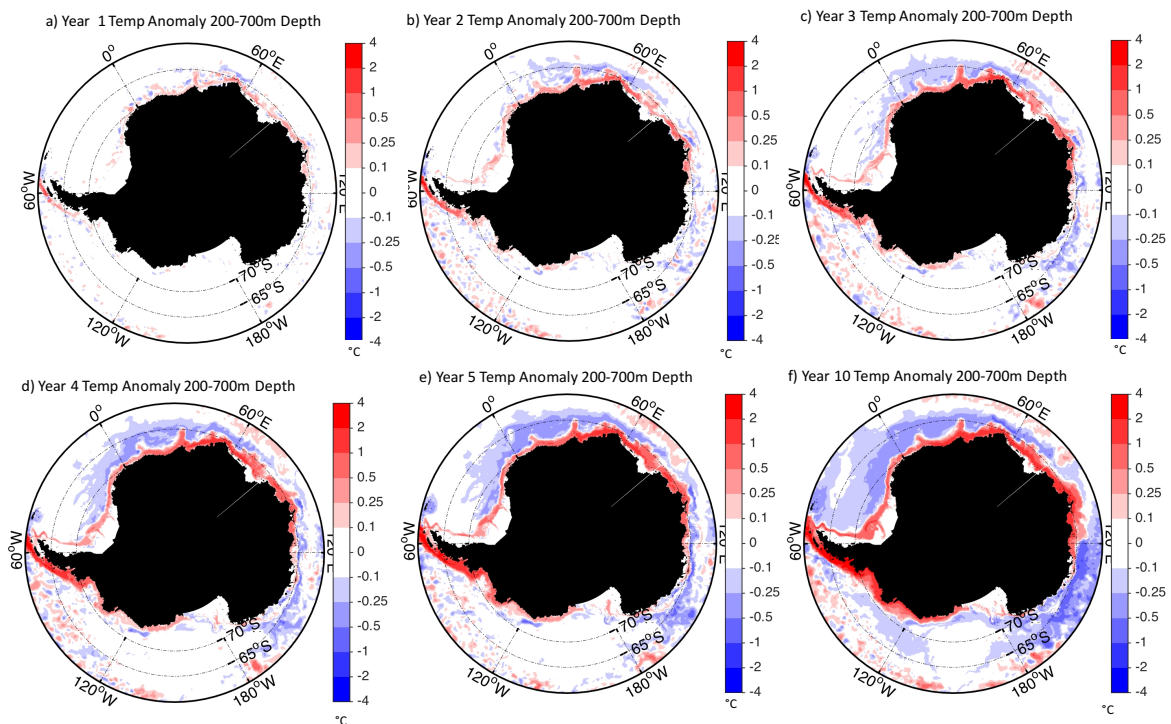
642 zonal mean sea-level pressure at the latitude closest to 65°S from the zonal mean sea-level

643 pressure at the latitude closest to 40°S. We use the CORE-II sea-level pressure and 10m

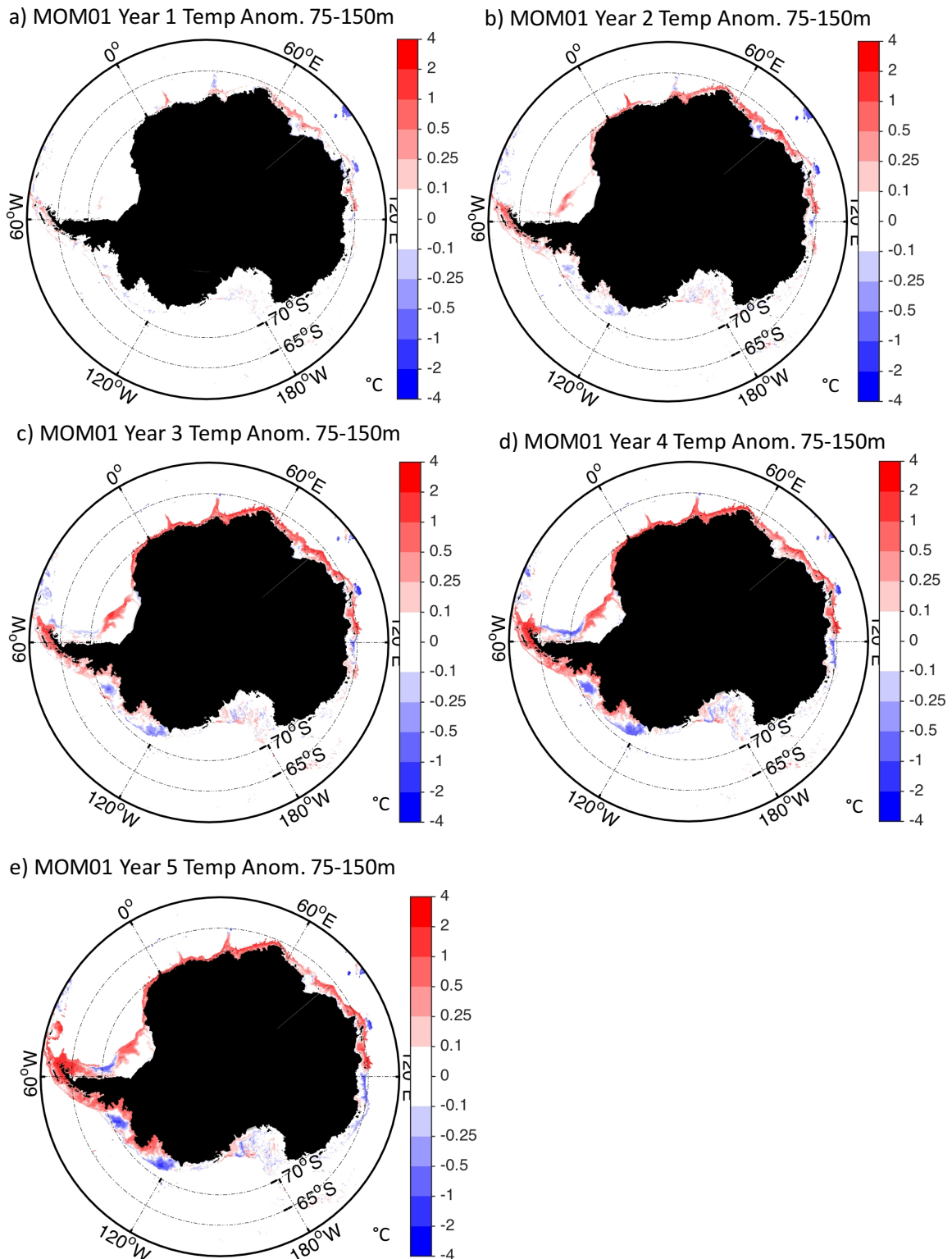
644 winds over 1948-2007³⁷. We use 74 CMIP5 simulations covering 1850 to 2100

645 ("historical" run over 1850-2005 and "RCP8.5" scenario over 2006-2100). The JFM

646 regressions are plotted as the mean of the three regression maps (Jan, Feb, Mar), and
647 similarly for JAS. The solid black lines in the bottom panels show the zonal boundaries of
648 the wind perturbation region.



649 **Supplementary Figure 2 | MOM025 Annual mean subsurface temperature response**
 650 **to East Antarctic poleward intensifying winds. Annual mean ocean temperature (°C)**
 651 **anomaly averaged between 200-700m depth in years 1, 2, 3, 4, 5 and 10 of the wind**
 652 **perturbation simulation. Note the non-linear color scale.**
 653



654

655

Supplementary Figure 3 | MOM01 Annual mean subsurface temperature response

656

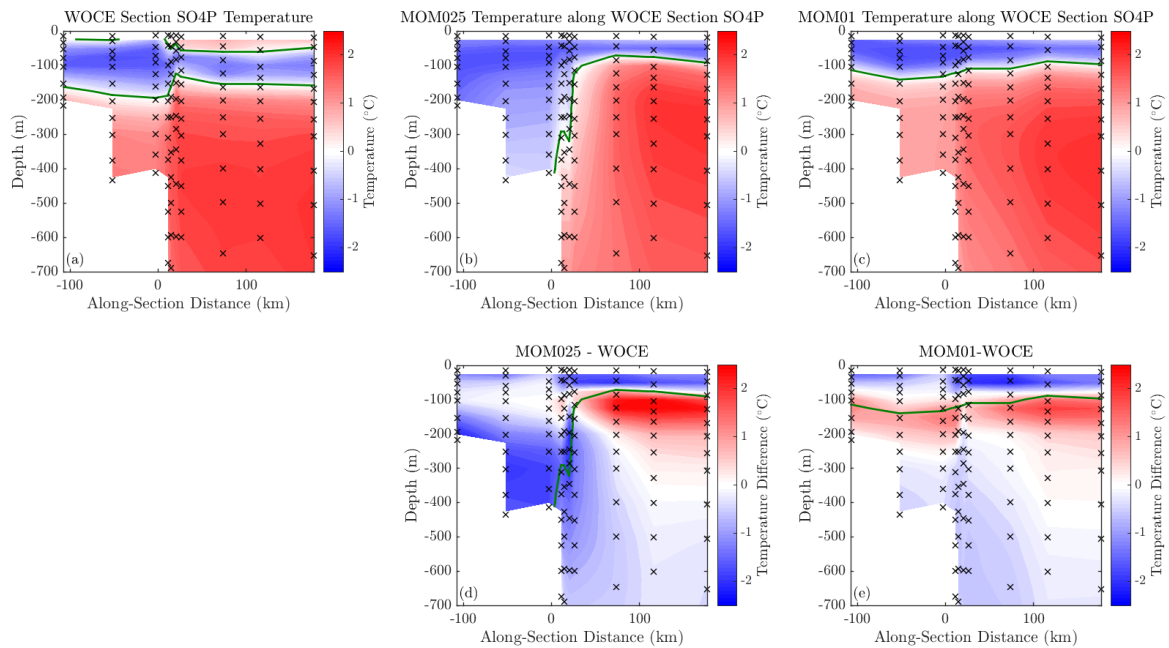
to East Antarctic poleward intensifying winds. Annual mean ocean temperature (°C)

657

anomaly averaged between 75-150m depth in years 1, 2, 3, 4, and 5 of the wind

658

perturbation. Note the non-linear color scale. Regions with depths >2000m are masked.



659

660 **Supplementary Figure 4 | Ocean temperature along hydrographic observation line**

661 **SO4P.** (a) Summer time hydrographic observations of temperature (°C) from the World

662 Ocean Circulation Experiment line SO4P³¹. Annual mean temperature in the unperturbed

663 state of (b) MOM025 and (c) MOM01 along line SO4P. Temperature difference between

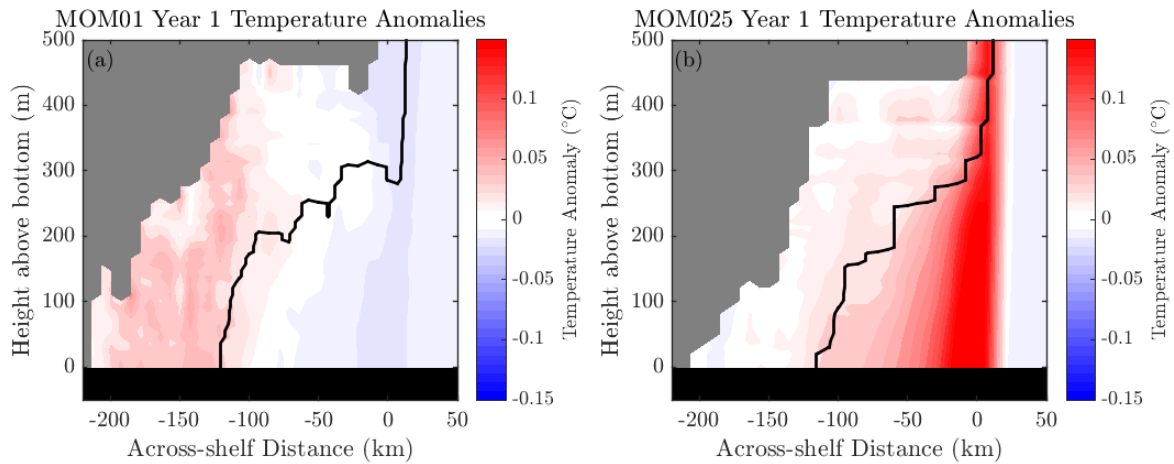
664 the hydrographic observations and (d) MOM025 and (e) MOM01 along the SO4P line.

665 The hydrographic line is on the western side of the Antarctic Peninsula as shown in Fig.

666 4a. The thick green lines show the position of the 0°C isotherm. The black symbols

667 indicate the location of the hydrographic measurements and where the corresponding

668 model temperatures were sampled.



670

671 **Supplementary Figure 5 | Across-shelf transects of temperature anomaly as a**672 **function of depth above the seafloor on the western side of peninsula in response to**673 **East Antarctic wind perturbation. Year 1 ensemble average temperature anomalies for**

674 (a) MOM01 and (b) MOM025 plotted with the distance above the seafloor on the y-axis.

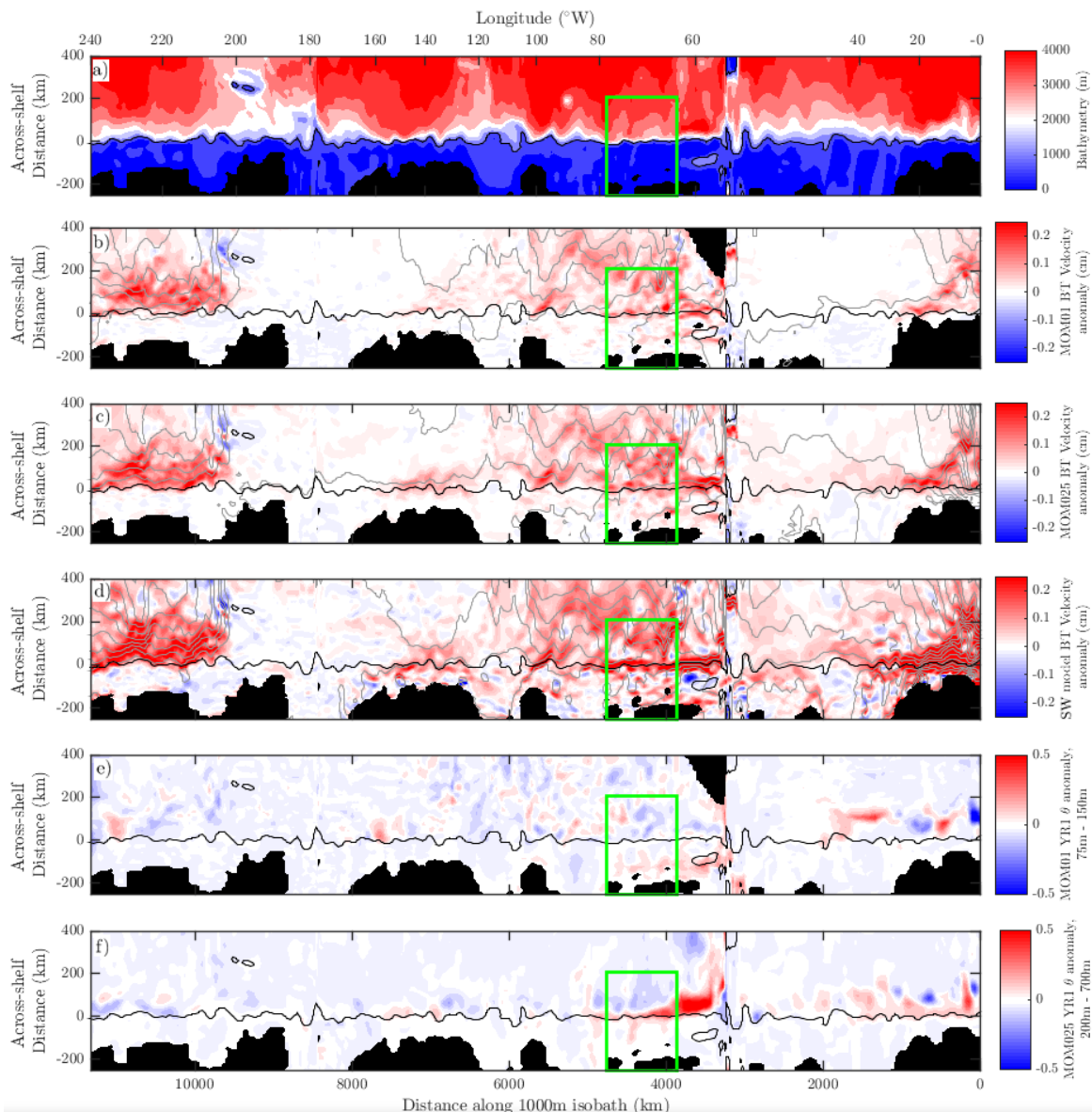
675 Compare with Fig. 4e,f where the anomalies are plotted with depth on the y-axis. The grey

676 region indicates where less than 20% of the data at that x-z location were within the ocean.

677 The thin black line indicates where 90% of the data at that x-z location were within the

678 ocean. The across-shelf-depth slice anomalies are averaged along the shelf within the

679 green region in Fig. 4a.



680

681 **Supplementary Figure 6 | Simulated across-shelf Antarctic coastal ocean properties.**

682 The smoothed 1000 m isobath is used to transform properties into an across- and along-

683 isobath coordinate system. (a) Bathymetry in the $1/4^\circ$ global ocean sea ice model. The

684 1000m and 2500m contours are highlighted with black contour lines, and the 1000m

685 contour is shown in each panel below. The bottom x-axis shows the distance (km) along

686 the contour and the top x-axis shows the approximate longitude position along contour. (b)

687 MOM01 wind perturbation day 5-15 average along-shelf barotropic velocity anomaly

688 (cm/s). (c) MOM025 day 5-15 average along-shelf barotropic velocity anomaly (cm/s). (d)

689 Day 5-15 average along-shelf barotropic velocity anomaly (cm/s) in a single-layer

690 shallow-water model that undergoes the same East Antarctic wind perturbation. (e)
691 MOM01 wind perturbation year 1 ensemble average temperature anomaly ($^{\circ}\text{C}$) averaged
692 from 75-150m depth. (f) MOM025 year 1 ensemble temperature anomaly ($^{\circ}\text{C}$) averaged
693 from 200-700m depth. The green box indicates the section on the western side of the West
694 Antarctic Peninsula shown in Figure 4. Data north of 60°S is not shown in panels b and e.
695
696